A multi-modal computational fluid dynamics model of left atrial fibrillation haemodynamics validated with 4D flow MRI

Louis Parker, Emilie Bollache, Shannon Soulez, Khaoula Bouazizi, Nicolas Badenco, Daniel Giese, Estelle Gandjbakhch, Alban Redheuil, Mikael Laredo, Nadjia Kachenoura

Original Research

A Multi-modal Computational Fluid Dynamics Model of Left Atrial Fibrillation Haemodynamics Validated with 4D flow MRI

Louis Parker PhD[1,2,3], Emilie Bollache PhD[1,2], Shannon Soulez MS[1,2], Khaoula Bouazizi PhD[1,2], Nicolas Badenco MD[2,4], Daniel Giese[5], Estelle Gandjbakhch MD PhD[2,4], Alban Redheuil MD, PhD[1,2,6], Mikael Laredo MD PhD[1,2,4], Nadjia Kachenoura PhD[1,2].

1. Laboratoire d'Imagerie Biomédicale (LIB), Sorbonne Université, Institut National de la Recherche Médicale (INSERM), Centre National de la Recherche Scientifique (CNRS), Paris, France.
2. ICAN Imaging, Institute of Cardiometabolism and Nutrition (ICAN), Paris, France.
3. School of Engineering, University of Western Australia, Perth, Australia.
4. Unité de Rythmologie, Institut de Cardiologie, Sorbonne Université, AP-HP, Hôpital Universitaire Pitié-Salpêtrière, Paris, France.
5. Magnetic Resonance, Siemens Healthineers AG, Erlangen, Germany.
6. Unité d'Imagerie Cardiovasculaire et Thoracique (ICT), Pitié-Salpêtrière Hospital, Paris, France.

Word Count: 250 (abstract), 3,972 (body).

Corresponding Author: Dr. Nadjia Kachenoura

Email: nadjia.kachenoura@inserm.fr

Abstract

Atrial fibrillation (AF) is characterized by rapid and irregular contraction of the left atrium (LA). Impacting LA haemodynamics, this increases the risk of thrombi development and stroke. Flow conditions preceding stroke in these patients are not well defined, partly due the limited resolution of 4D flow magnetic resonance imaging (MRI). In this study, we combine a high-resolution computed tomography (CT) LA reconstruction with motion and pulmonary inflows from 4D flow MRI to create a novel multimodal computational fluid dynamics (CFD) model, applying it to five AF patients imaged in sinus rhythm (24±39 days between acquisitions). The dynamic model was compared with a rigid wall equivalent and the main flow structures were validated with 4D flow MRI. Point-by-point absolute differences between the velocity fields showed moderate differences given the sensitivity to registration. The rigid wall model significantly underestimated LA time-averaged wall shear stress (TAWSS) ($p=0.02$) and oscillatory shear index (OSI) ($p=0.02$) compared to the morphing model. Similarly, in the left atrial appendage (LAA), TAWSS ($p=0.003$) and OSI ($p<0.001$) were further underestimated. The morphing model yielded a more accurate mitral valve waveform and showed low TAWSS and high OSI in the LAA, both associated with thrombus formation. We also observed a positive correlation between indexed LA volume and endothelial cell activation potential (ECAP) ($R^2=0.83$), as well as LAA volume and LAA OSI ($R^2=0.70$). This work demonstrates the importance of LA motion in modelling LAA flow. Assessed in larger cohorts, LAA haemodynamic analysis may be beneficial to refine stroke risk assessment for AF.

Keywords: Atrial fibrillation, computational fluid dynamics, hemodynamics, multi-modal, fluid mechanics.

Background

Atrial fibrillation (AF) is a cardiac arrythmia characterized by abnormal contraction of the atrium. It is caused by the disturbed propagation of electrical signals across the atrial myocardium.[1] Incidence of AF has been rising steadily with the worldwide prevalence increasing by 33% since 2000.[1] AF patients are at a 3-5 fold increased risk of stroke[2,3] as well as elevated risk of heart failure and all-cause mortality.[4] Over 90% of the thrombi responsible for stroke in AF originate in the left atrial appendage (LAA) where haemodynamic conditions are often pro-thrombotic.[5] Low wall shear stress (WSS) and high oscillatory shear index (OSI) resulting from stagnant, disordered and time-varying flow, are considered pro-thrombotic as they interfere with normal endothelial function.[6–8] Originally developed in the setting of abdominal aortic aneurysms[9], endothelial cell activation potential (ECAP), which combines these two characteristics into a single metric (OSI/time-averaged WSS), has recently been used to further characterize disturbed flow in the LAA.[6,6,10] Treatment options for AF include catheter ablation whereby the atrial wall is selectively scarred to interrupt stray electrical signals and restore sinus rhythm. Anticoagulants are also usually prescribed to AF patients with risk factors to mitigate stroke risk.[11]

Magnetic resonance imaging (MRI) is well suited for tissue characterisation in the diagnosis and monitoring of heart disease.[12] Further developments allowing the volumetric encoding of intra-cardiac blood flow velocity in 3D and throughout the cardiac cycle (4D flow) have made MRI a powerful tool in the assessment of cardiac flow.[13–16] Although its use in routine clinical practice is not widespread, 4D flow MRI has furthered our understanding of the interplay between left atrial (LA) flow and AF.[17–19] Whilst 4D flow MRI offers direct measurement of blood flow velocities, the relatively low spatial resolution presents challenges. WSS estimation requires accurate assessment of the near-wall velocity gradient. With 4D flow,

WSS must be approximated by interpolation between the wall and the noisy near-wall velocities introducing significant error.[20,21] Conversely, computational fluid dynamics (CFD) meshes can provide highly-resolved WSS fields. Such models have been widely used in vascular disease to predict disease progression.[22–25] Increasingly, CFD methods are being employed to characterize LA flows in AF.[26–29] These studies have typically assumed the LA wall to be rigid. Whilst some studies have applied multiphase computed tomography (CT) to dynamically deform the LA in CFD simulations,[30–32] no CFD study has yet extracted LA motion and pulmonary veins (PV) inflows from the same MRI acquisition.

The aim of this study was to develop a multi-modal, dynamic CFD model to produce patient-specific LA haemodynamic data in higher temporal and spatial resolution than current imaging methods offer. This model was then applied to a small cohort of AF patients to assess existing theories and generate new hypotheses as to the genesis of stroke in these patients.

Methods

This study was based on retrospective analysis of five patients (Table 1) from the CTStrain-AF Study (NCT04281329), an observational study administered by Assistance Publique - Hôpitaux de Paris and approved by institutional review board. All participants were scheduled for their first radiofrequency ablation in the next 6 months, were ≥18 years of age and gave written informed consent for participation in the study. All patients analysed in the present study were imaged at Centre Hospitalier Universitaire Pitié-Salpêtrière in Paris. In addition to a routine cardiac CT scan, these patients received MRI with 4D flow, encompassing the whole heart, prior to catheter ablation. These two datasets were used to create a multimodal model of the LA (Figure 1). The patients were imaged whilst in sinus rhythm and the mean delay between CT and 4D flow MRI acquisitions was 24±39 days

Table 1. Patient characteristics.

Case	Sex	Age (yrs)	Weight (kg)	Height (cm)	BSA (m^2)	HR (BPM)	CO (L/min)	LAEF (%)	LA indexed volume (mL/m^2)	LAA volume (mL)
1	F	64	69	165	1.76	50	3.4	24.4	63.1	6.7
2	M	76	74	170	1.85	68	3.6	20.2	82.8	6.7
3	F	71	59	158	1.60	48	2.7	22.6	41.6	3.9
4	M	61	84	180	2.04	67	5.1	29.1	45.6	4.6
5	M	71	80	178	1.98	56	3.8	39.3	50.8	5.3

Note: BSA = body surface area, HR = heartrate, BPM = beats per minute, CO = cardiac output, LAEF = left atrial ejection fraction, LA = left atrium, LAA = left atrial appendage, F = female, M = male.

3D geometric model reconstruction from CT data

The 3D geometric models of the LA were based on the CT data given its high spatial resolution. Such data were acquired on a Siemens SOMATOM Force dual-detector CT scanner with a pixel spacing of 0.35-0.47 mm and slice thickness of 0.6 mm. Acquisitions were made either at peak systole (cases 1-4) or diastole (case 5). Reconstruction was then achieved via manual thresholding within 3D Slicer (Version 5.2.1). The stereolithography (.STL) file was then exported to Star CCM+ (Version 2022.1, Siemens, Munich) where local smoothing was used to remove any imaging or segmentation artefacts.

4D flow MRI acquisitions

MRI images were acquired on a 1.5T scanner (MAGNETOM Sola, Siemens Healthineers, Erlangen, Germany). Phase-contrast MRI with 3D velocity-encoding throughout the cardiac cycle was obtained for all patients using a 4D flow MRI research sequence.[33] Images were acquired during free-breathing with respiratory navigator and retrospective electrocardiogram (ECG) gating in a sagittal oblique volume encompassing the left heart, using the following scan parameters: echo time (TE) = 2-2.25 ms, repetition time (TR) = 4.33 ms, average temporal

resolution = 26.0 ms, views per segment = 2, flip angle = 7°, reconstructed pixel spacing = 2.4 x 2.4 mm^2, slice thickness = 3 mm, reconstructed 25-phase volumes, accelerated using compressed sensing with an acceleration factor of R=7.7. Optimal single encoding velocity (VENC) in all spatial directions is set according to scout in-plane velocity-encoded images acquired in a 3-chamber view just before 4D flow scans. As such, VENC was 150 cm/s for Cases 1-4. For Case 5 VENC was 300 cm/s due to the presence of aortic valve stenosis resulting in high velocities and thus aliasing in the aortic root as revealed by scout images acquired at VENC = 150 and then 200 cm/s.

LA dynamic wall motion from MRI

The SegmentRegistration module[34] available within 3D Slicer, which extends the previous Elastix tool to temporal sequences,[35,36] was used to generate a series of transforms describing transient LA motion from 4D flow MRI magnitude images (Figure S1). The corresponding CT reconstruction was then manually registered to the MRI (and transform sequence) coordinate system. To implement these transforms in Star-CCM+, a grid of 125 control points was generated in 3D Slicer across the spatial range of the LA and a time-position table for each of these points was exported. Within Star-CCM+ these control points were implemented with B-spline interpolation to morph the computational mesh. All cases were also simulated with rigid walls, based on the original CT reconstruction, to assess the sensitivity of the haemodynamic results to rigid vs. moving wall assumption.

Extraction of PV inflow, mitral outflow and model validation from MRI

PV inflows and mitral valve outflow were quantified in Medis Suite MR (version 4.0, Medis Medical Imaging, Leiden) by re-slicing the 3D image stack into 2D planes perpendicular to each PV and to the mitral valve, respectively, extracting the contour of interest and calculating

the time-resolved flow rate profile. PV flow rate profiles were then imported into Star-CCM+ where a spline interpolation was used to specify time dependant boundary flows. In parallel, the raw 4D flow velocity images were post-processed in MATLAB into a series of velocity-position tables for each phase of the cardiac cycle. Such tables were imported into Star-CCM+ to compare with the CFD velocity field and validate the major flow structures in the LA throughout the cardiac cycle.

CFD model

Second-order transient simulations were run with Star-CCM+'s laminar flow model and a constant timestep of 0.001 s for a total of 5 cardiac cycles. The computational meshes were based on the CT reconstructions and were constructed with a polyhedral core mesh and 12 prismatic boundary layers. Fifteen-cm extrusions were made to the inlets to create a fully-developed flow profile. The mitral valve for all cases was modelled as fully open with zero pressure. The outlet waveform was therefore a result of the total pulmonary inflow and the change in LA volume. To assess mesh convergence, three meshes of varying densities (0.74M, 1.45M and 2.76M cells) were compared for Case 1. Once an appropriate degree of mesh refinement was established (2.76M cells, mean mesh size = 0.4 mm, the same meshing parameters were applied to all cases. Time-averaged velocity was assessed on two-line probes of 50 points each spanning the LA/LAA horizontally and vertically (Figure S2) and throughout the entire LA (Figure S3/S4). Time-averaged WSS (TAWSS) was assessed as a surface average across the entire LA surface (Figures S5/6). TAWSS, OSI and ECAP were extracted from the final cardiac cycle using a 100-sample sliding window. Blood density was 1050 kg/m^3 and a non-Newtonian, Carreau-Yasuda blood viscosity model (haematocrit=45%) was used.[37] The simulations were run on the MeSU supercomputer (Sorbonne Université) on 96 cores with a mean simulation time of 7 hours and 10 mins. In our analysis of the haemodynamic data we

refer to indexed LA volumes which were calculated by dividing late systole (maximum) LA volume by body surface area (BSA). BSA was calculated according to the Du Bois formula.[38]

Statistical Analysis

Continuous variables were provided as mean (standard deviation, SD). To compare haemodynamic differences between the LA and LAA as well as between rigid and morphing models, a two-tailed paired t-test was performed with the normality of the data confirmed using a Shapiro-Wilk test. Finally, associations of TAWSS, OSI and ECAP with LA and LAA volumes were studied using linear regressions. R^2 Pearson correlation coefficients were provided. Statistical analyses were performed using Real Statistics Resource Pack for Excel (Microsoft, Redmond).

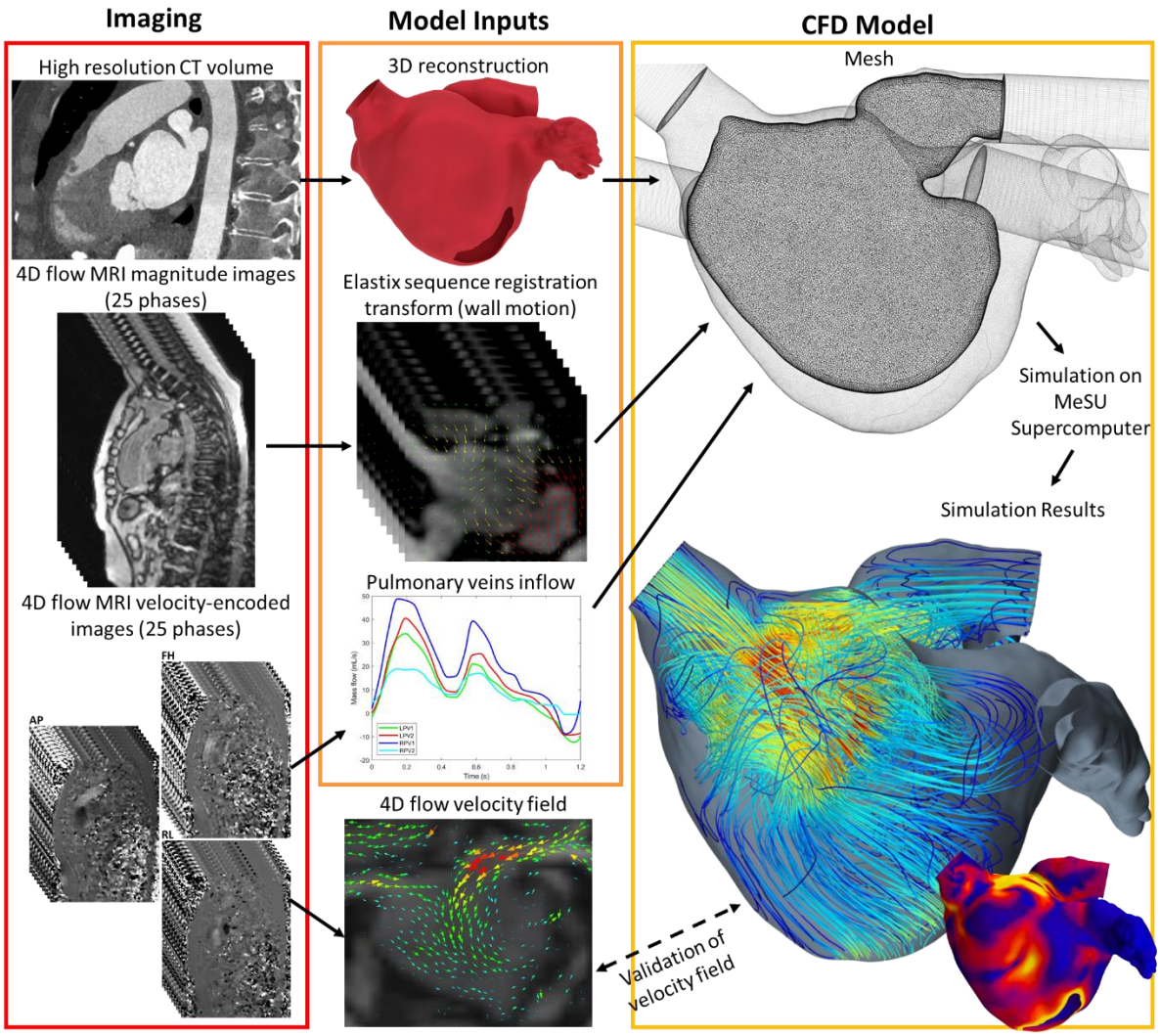

Figure 1. The workflow from imaging data to simulated haemodynamic results. AP: antero-posterior, FH: foot-head and RL: right-left directions.

Results

Grid convergence was acceptable for velocity (Figures S2 to S4) and TAWSS (Figures S5/6) on the finest mesh (2.76M cells, mean mesh size = 0.4 mm). Time-averaged velocity across the two-line probes and averaged across the entire LA volume differed by <1% when comparing the medium and fine mesh results, whilst TAWSS differed by 0.9% in the LA and 3.0% in the LAA where TAWSS was very low.

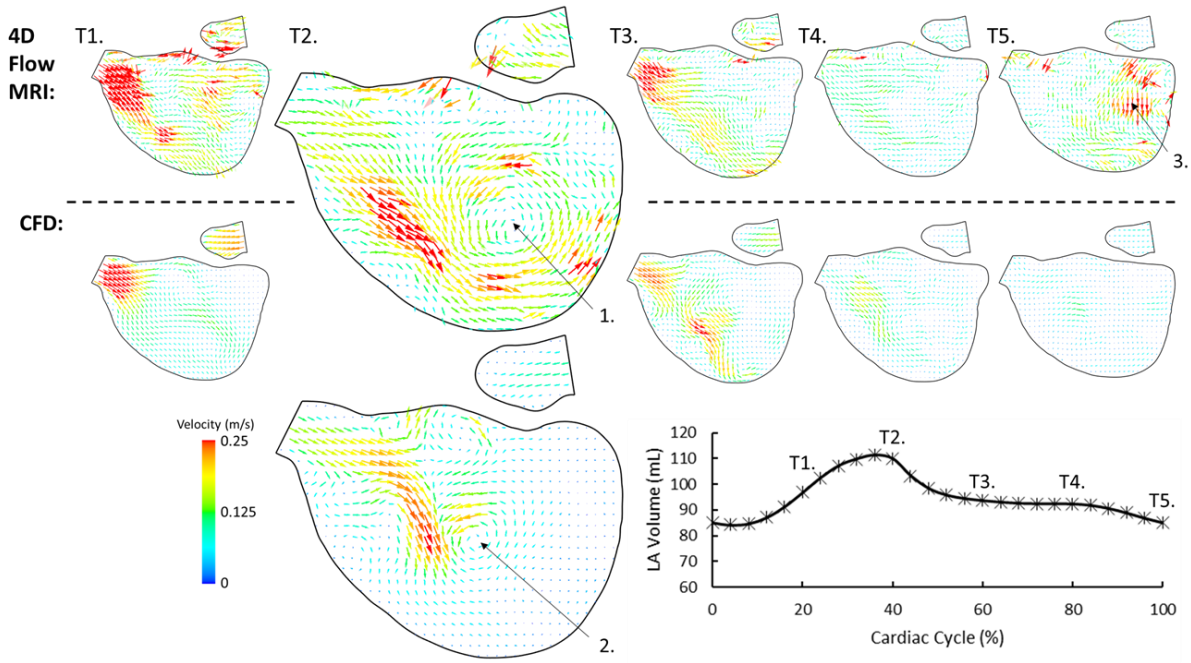

191

192 **Figure 2. Validation of the CFD velocity field against 4D flow MRI data in Case 1.** 4D
193 flow MRI (upper row) and CFD (lower row)-derived instantaneous velocity vectors on a plane
194 through the left atrium (LA) for five temporal positions (T1-T5). These timepoints are indicated
195 on the left atrium volume curve (bottom right). Points 1 and 2 show a large vortex in the LA
196 whilst point 3 indicates noisy velocity vectors.

197

198 **Table 2.** Mean and standard deviation (SD) absolute velocity error (m/s) between CFD and 4D
199 flow MRI velocity fields in the left atrium for the five cases.

	Systole		**Diastole**	
	Mean	SD	Mean	SD
Case 1	0.07	0.05	0.05	0.05
Case 2	0.05	0.05	0.04	0.03
Case 3	0.05	0.04	0.06	0.05
Case 4	0.05	0.05	0.05	0.04
Case 5	0.08	0.07	0.05	0.05
Mean	0.06	-	0.05	-
SD	0.06	-	0.05	-

200

Comparison of the 4D flow and CFD temporal velocity fields for Case 1 shows good agreement with the same large-scale structures observed in each (Figure 2, points 1 & 2). Towards time point T5, when the LA empties and contracts towards its minimum volume, the 4D flow shows some large, incongruous velocity vectors (Figure 2, point 3) likely arising from noise exterior to the LA in the surrounding tissue. A visual comparison of the flow fields in all cases at systole and diastole is shown in the supplemental material (Figure S7) with reasonable agreement. Point-by-point absolute difference between the 4D flow MRI and CFD velocity fields are reported in Table 2 for all five cases, revealing moderate differences given the sensitivity to registration between the two fields. Of note, Case 5, which had a higher encoding velocity (300 cm/s), showed the highest systolic velocity errors.

Comparing the rigid and morphing models (Figure 3) revealed that the rigid model significantly underestimated LA TAWSS (mean±SD=0.51±0.14 Pa vs. 0.63±0.16 Pa, $p=0.02$) and OSI (mean±SD=0.18±0.01 Pa vs. 0.23±0.03 Pa, $p=0.02$) compared to the morphing model across the five cases. In the LAA, TAWSS (mean±SD=0.05±0.02 Pa vs. 0.21±0.05 Pa, $p=0.003$) and OSI (mean±SD=0.25±0.04 Pa vs. 0.42±0.03 Pa, $p<0.001$) were also underestimated though to a far greater degree. Looking at the mitral valve outflow for all cases (Figure 4), the rigid wall assumption decreased E and A wave amplitudes by an average of 44% and 46%, respectively, when compared to the 4D flow MRI measurements. The morphing model also showed decreases in E and A wave amplitude of 14% and 48%, respectively, indicating a considerably improved E wave estimation (Supplemental material, Table S1) and slightly worse A wave.

223

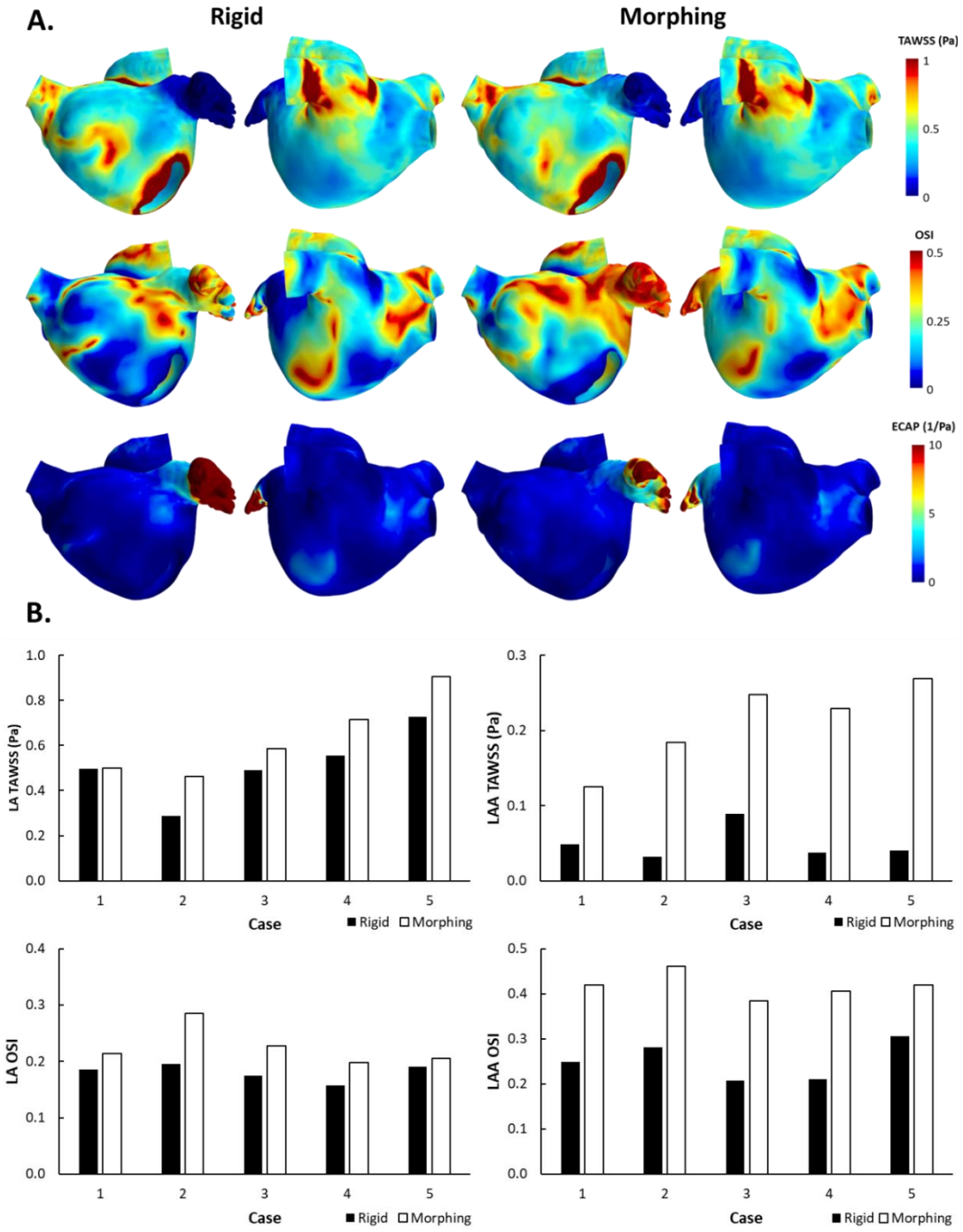

224 **Figure 3. A.** Time-averaged wall shear stress (TAWSS), oscillatory shear index (OSI) and
225 endothelial cell activation potential (ECAP) in the rigid and morphing models (Case 1). **B.**
226 Quantitative comparison of surface-averaged TAWSS (top row) and OSI (bottom row)
227 between rigid and morphing models in the left atrium (LA) and left atrial appendage (LAA)
228 for the 5 cases analysed.

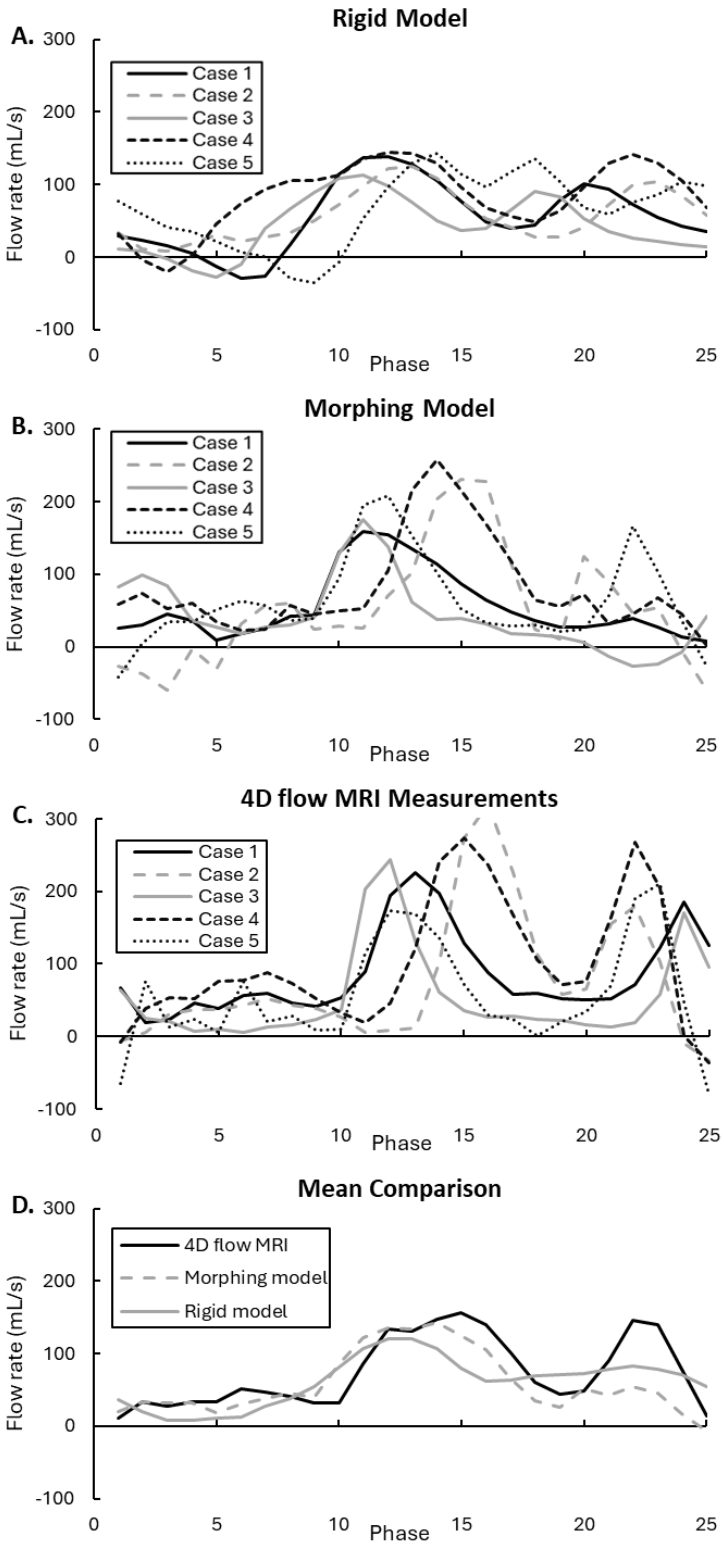

Figure 4. The mitral valve outflow obtained from the rigid computational fluid dynamics (CFD) model (**A.**), the morphing CFD model (**B.**) and as measured from 4D flow magnetic resonance imaging (MRI) (**C**.). **D.** Mitral outflows for the data in A, B and C averaged across all 5 cases. All waveforms are plotted across the 25 MRI time-phases.

The haemodynamic results from the morphing model (Table 3) show that the LAA exhibits substantially lower TAWSS (-66±6%, p=0.003), along with higher OSI (87±18%, p=<0.001) and ECAP (531±192%, p=0.01) compared to the LA (Figure 5/6A). Haemodynamic metrics were plotted against indexed LA/LAA volume (Figure 6B), indicating that increased indexed end-systolic LA volume was correlated with decreased TAWSS (R^2=0.35) as well as increased OSI (R^2=0.65) and ECAP (R^2=0.83). Similarly, increased LAA volume was associated with decreased TAWSS (R^2=0.61) and increased OSI (R^2=0.70) and ECAP (R^2=0.51).

Table 3. Surface-averaged haemodynamic results for the left atrium (LA) and the left atrial appendage (LAA).

	TAWSS (Pa)		OSI		ECAP (1/Pa)	
Case	**LA**	**LAA**	**LA**	**LAA**	**LA**	**LAA**
1	0.50 (0.38)	0.12 (0.09)	0.21 (0.11)	0.42 (0.05)	0.60 (0.46)	5.71 (4.34)
2	0.46 (0.40)	0.18 (0.10)	0.29 (0.11)	0.46 (0.03)	0.84 (0.50)	3.20 (1.62)
3	0.59 (0.25)	0.25 (0.15)	0.23 (0.12)	0.38 (0.12)	0.48 (0.34)	2.35 (1.72)
4	0.71 (0.40)	0.23 (0.12)	0.20 (0.10)	0.41 (0.09)	0.36 (0.27)	2.49 (1.79)
5	0.90 (0.68)	0.27 (0.15)	0.21 (0.10)	0.42 (0.07)	0.35 (0.47)	2.22 (1.72)
Mean (SD)	0.63 (0.18)	0.21 (0.06)	0.23 (0.03)	0.42 (0.03)	0.52 (0.20)	3.20 (1.46)

Note: TAWSS = time-averaged wall shear stress, OSI = oscillatory shear index, ECAP = endothelial cell activation potential, LA = left atrium, LAA = left atrial appendage, SD = standard deviation.

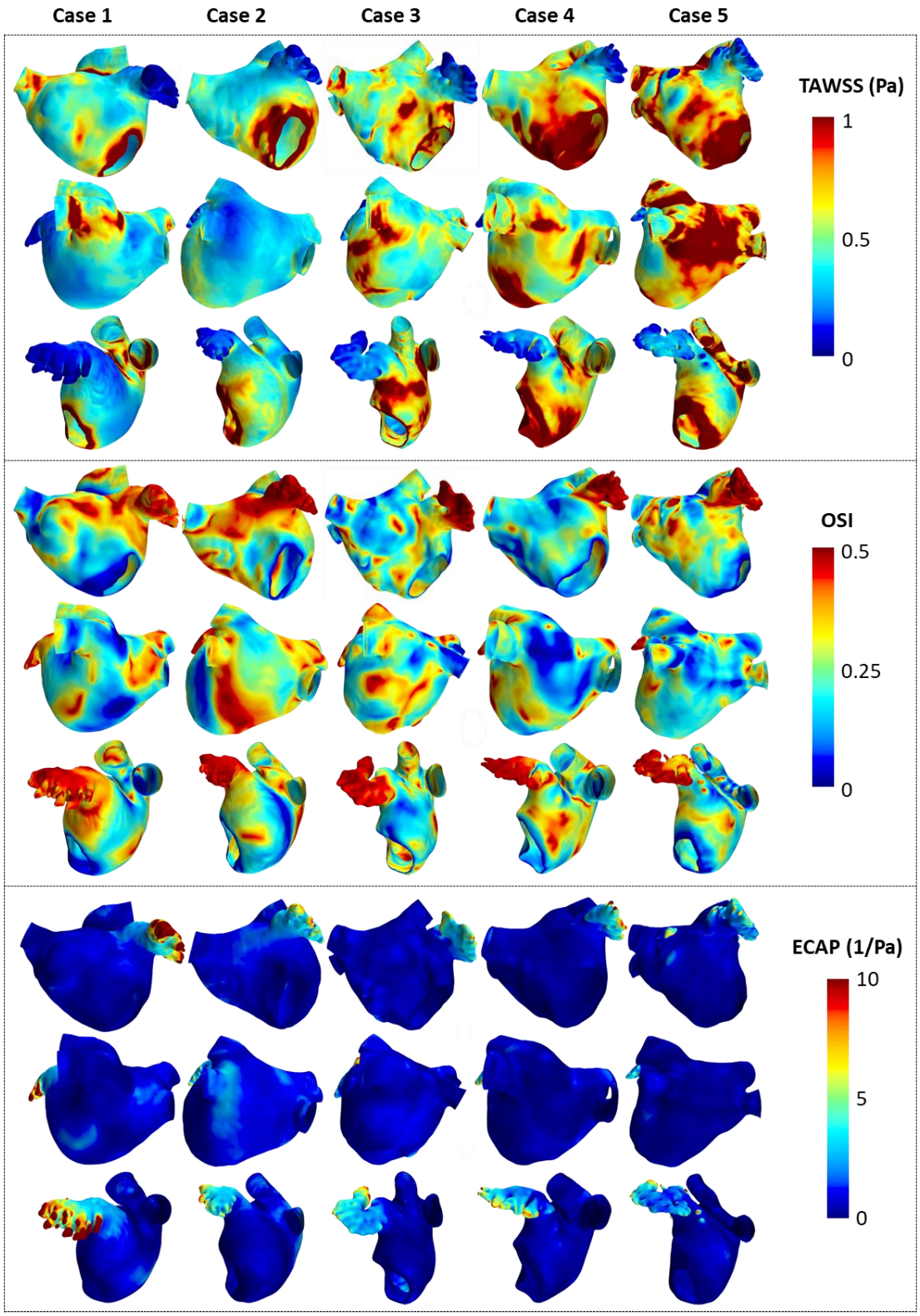

Figure 5. Left atrial time-averaged wall shear stress (TAWSS), oscillatory shear index (OSI) and endothelial cell activation potential (ECAP) for cases 1-5 in the anterior (top), posterior (middle) and lateral views (bottom).

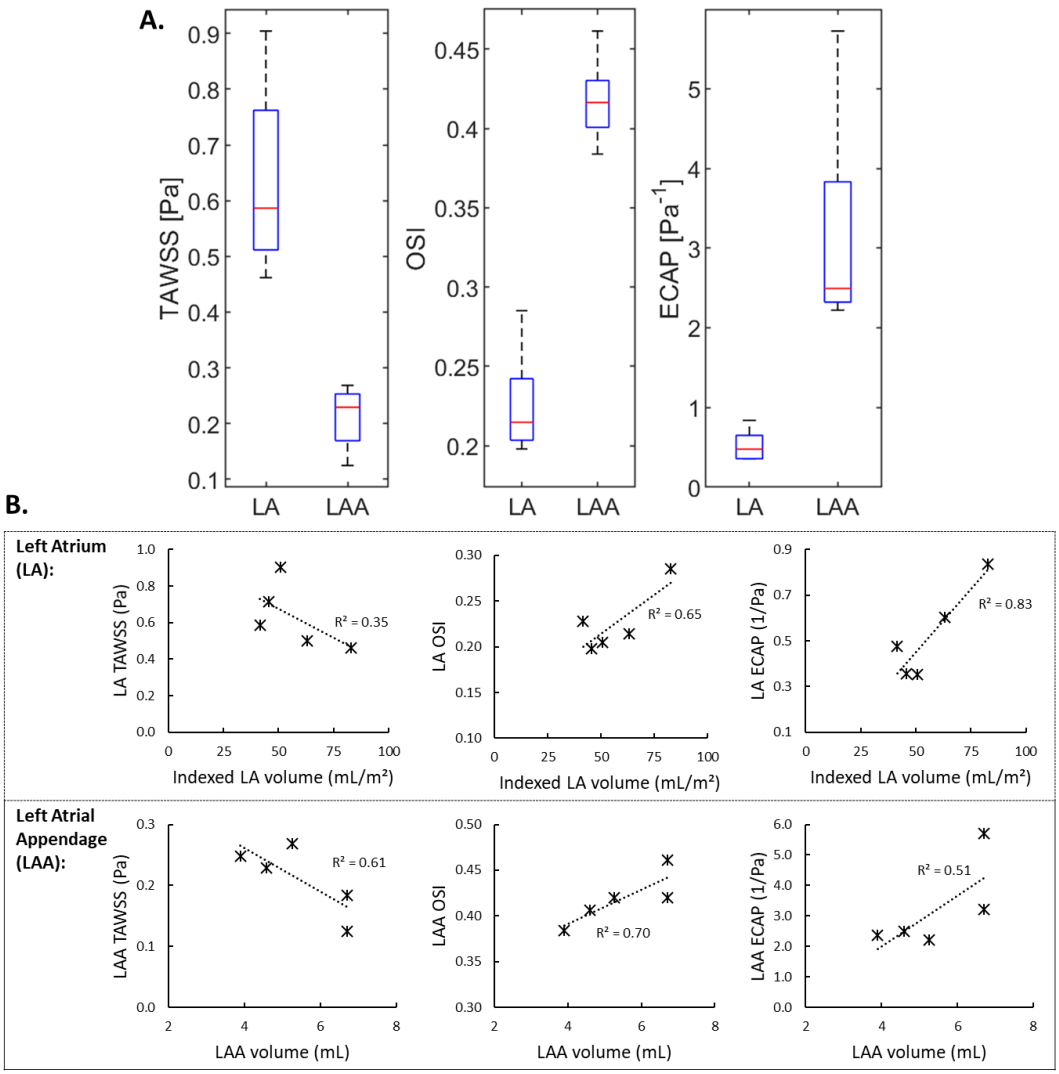

Figure 6. A. Time-averaged wall shear stress (TAWSS), oscillatory shear index (OSI) and endothelial cell activation potential (ECAP) surface-averages for the left atrium (LA) and left atrial appendage (LAA). **B.** Linear regressions along with correlations between the haemodynamic metrics presented in A and indexed end-systolic LA volume (top) and LAA volume (bottom).

Discussion

In this study we present a novel multi-modal CFD model for the left atrium. The need for such a model comes from the relatively low resolution of 4D flow MRI, along with its implications

for WSS estimation[39] and the well-established link between WSS and thrombosis.[40,41] This is particularly important in the LAA where 4D flow analysis is challenging.[42] We first outline the accuracy and suitability of our novel CFD model of the LA. We then analyse results from a small group of AF patients to examine existing hypotheses about thrombi formation and describe potential new relationships between LA/LAA volumes and haemodynamic indices.

Left atrium CFD model

We present here, to the authors best knowledge, the first comparison of a LA CFD model with 4D flow MRI (Figure 2/S7, Table 2). Whilst these results are highly sensitive to cross-sectional plane positioning, we see the same large-scale structures (Figure 2, pts 1. & 2). These results are encouraging evidence that our CFD model accurately characterises such structures. Noisy velocity vectors are a common issue with 4D flow MRI especially in enlarged LAs where the velocity-to-noise ratio is lower. Such noise was observed in some cases (Case 1 Figure 2 pt. 3, Case 5 Figure S7). This highlights another benefit of the CFD model which is free from imaging noise and underpins the need to use the lowest practical encoding velocity.

The resolution offered by CT is critical to capture the intricate and highly patient-specific morphology of the LA and especially of the LAA. For this reason it has been the basis of the 3D reconstruction for the majority of CFD studies.[31,43–45] The novel aspect of the present study was to then register the CT geometric reconstruction to a MRI dynamic sequence applying patient-specific PV inflows and LA wall motion. PV inflow distribution has been previously shown to impact atrial flows,[46,47]; whilst it is common to assume an even distribution, here we applied unique patient-specific waveforms from 4D flow MRI to each PV. Similarly, the vast majority of previous CFD studies have assumed a rigid wall boundary condition, citing the reduced LA function in AF patients.[48,49] Whilst LA ejection fraction may be impeded in these patients it is not necessarily indicative of negligible local wall motion for

287 both the LA driven phases (reservoir and contraction) and the ventricular-driven phase
288 (conduit). Several CFD studies have however incorporated dynamic LA motion. Some applied
289 a generic or measured mitral valve annulus motion,[27,50] a synthetic global displacement[51] or a
290 similar approach to the present study, extracting local displacements from multiphase MRI or
291 CT.[31,52] Our results show that haemodynamic indices vary significantly between rigid and
292 morphing models (Figure 3). The impact is greatest in the LAA, supporting recent findings,[53]
293 where the rigid model fails to capture the oscillatory nature of the flow and records near-zero
294 TAWSS in some regions, the latter causing ECAP to be greatly overestimated. These results
295 make logical sense with wall motion being critical to flushing out stagnant pockets in the
296 intricate structure of the LAA.

297 Further to this, we have compared the impact on mitral valve outflows (Figure 4). Due
298 to conservation of mass (and volume for an incompressible fluid), mitral outflow is coupled to
299 changes in volume which are responsible for the characteristic E wave, occurring during LA
300 conduit phase, and A wave, occurring during LA contraction phase. An improved E wave
301 estimation was observed with the morphing model whilst A wave characterisation was slightly
302 worse. The consistent underestimation of the A wave may cause both models to underestimate
303 LA/LAA emptying and so overestimate the thrombogenicity. We see in the present study that
304 the amplitude and timing of the E wave is vastly improved when morphing the CFD model
305 (Figure 4B). Improvements to this registration algorithm will likely enhance the A wave. An
306 original feature of our approach is the inherent coupling of the wall motion and PV inflows,
307 both measured from the same MRI acquisition. Indeed, when motion and flow boundary
308 conditions are derived from separate acquisitions, like combining PV Doppler
309 echocardiography with dynamic CT, there is a greater risk of variability in the resultant mitral
310 valve outflow.

311

Haemodynamics of the left atrium and left atrial appendage

The model was applied to a small group of AF patients prior to ablation (Table 3, Figure 5). The haemodynamic results showed in all patients lower TAWSS in the LAA compared to the LA which has recently been associated with stroke.[54] Perhaps the most noteworthy result was the systematically elevated OSI values in the LAA, suggesting a stagnant LAA with no consistent flush-out. Such conditions, as per Virchow's triad, are pro-thrombotic.[41] Being a dynamic model, the LAA moves considerably throughout the cardiac cycle. As observed by Koizumi et al., high frequency fibrillation may increase LAA OSI.[27] These results might also explain why models which implement motion only via mitral valve longitudinal displacement have not reported increased OSI in the LAA of stroke patients.[50]

In our cohort, we saw a strong relationship between LAA volume and haemodynamics. Higher LAA volume was associated with pro-thrombotic conditions. LAA volume has previously been associated with stroke risk[55] and increased ECAP.[56] Like Lee et al.,[55] we also observed a strong relationship between orifice area and pro-thrombotic conditions (low TAWSS, R^2=0.93, Supp material Figure S8) though this may simply be emblematic of a larger LAA. Low WSS within the LAA is to be expected given its unique anatomy and has been observed in healthy subjects.[57] What the present study highlights, by comparing rigid wall and dynamic models, is that LAA OSI is closely related to motion. This motion may be unique to AF patients whereby the LAA is 'rattled' during fibrillation, increasing OSI and the occurrence of thrombosis in these patients.

Limitations

There are several limitations of this study. The registration of the 3D model reconstructed from CT to the MRI coordinate system is performed manually. As these are two separate acquisitions, there is never a perfect registration of the two datasets. The applied motion model

fixes the PV inlets in space throughout the cycle. This neglects the slight translation or change in dimension of these veins. 4D flow MRI signal-to-noise ratio (SNR) is lower than other sequences that may be better suited to motion quantification. The 4D flow field itself is also more prone to errors arising from low velocity-to-noise ratio (VNR), breathing motion artefacts, undersampling artefacts and heart cycle variations. For Case 5 the encoding velocity was higher than the remaining cases (300 cm/s vs. 150 cm/s). Results from this case are therefore more susceptible to errors arising from a low VNR, as VNR is proportional to 1/VENC.[58] Whilst 4D flow MRI provides validation of the flow in the LA itself, the resolution is too limited to provide a meaningful comparison in the LAA. 4D flow MRI measurements at the mitral valve used for validation are sensitive to motion tracking.[59] All patients were imaged whilst in sinus rhythm; analysis of patients during AF may be required to reveal the mechanisms of AF-related thrombus formation in the LAA. Acquiring 4D flow MRI during AF is challenging and 5D flow techniques, which further encodes the heart rhythm, may offer insights into such mechanisms.[60] Finally, the mitral valve is modelled as constantly open. Whilst the coupling of the PV inflows and wall motion (volume change) ensures a realistic transient flow through the valve, the shape of the valve is not distinguishable in the dynamic MRI and as this is an outlet it is likely to have very little impact on LA flow.

Conclusion

In this study we present a novel model of LA flow. We combine high-resolution CT with 4D flow MRI to create a high-resolution patient-specific dynamic model with PV inflows, validated against 4D flow MRI. We compare the performance of this model with results from a rigid wall simulation, revealing that the rigid model underestimates TAWSS and OSI, whilst substantially overestimating ECAP. We then apply this model to a group of five AF patients and show in the LAA the low TAWSS and high OSI/ECAP associated with thrombosis. Left

atrial volume appears to correlate with pro-thrombotic conditions in the LAA. Whilst rigid wall models are capable of capturing the low TAWSS in the LAA, we show here the advantage of a dynamic model in capturing high OSI which may, if confirmed in a large cohort, become an important clinical predictor of thrombosis.

Declarations

Compliance with Ethical Standards

Patients in the CTStrain-AF (NCT04281329) gave written informed consent for participation in the study.

Consent for publication

All participants provided consent for publication.

Funding

This project has received funding from the European Union's Horizon 2020 research and innovation programme under the Marie Skłodowska-Curie grant agreement No 101105768.

Acknowledgments

This work was granted access to the HPC resources of the SACADO MeSU platform at Sorbonne Université.

References

[1] G. Lippi, F. Sanchis-Gomar, and G. Cervellin, "Global epidemiology of atrial fibrillation: An increasing epidemic and public health challenge," International Journal of Stroke **16**(2), 217–221 (2021).

[2] P.A. Wolf, R.D. Abbott, and W.B. Kannel, "Atrial fibrillation as an independent risk factor for stroke: the Framingham Study," Stroke **22**(8), 983–988 (1991).

[3] P.A. Wolf, T.R. Dawber, Jr. Thomas H.E., and W.B. Kannel, "Epidemiologic assessment of chronic atrial fibrillation and risk of stroke: the Framingham study," Neurology **28**(10), 973–7 (1978).
[4] S. Stewart, C.L. Hart, D.J. Hole, and J.J.V. McMurray, "A population-based study of the long-term risks associated with atrial fibrillation: 20-year follow-up of the Renfrew/Paisley study," Am J Med **113**(5), 359–364 (2002).
[5] W.D. Johnson, A.K. Ganjoo, C.D. Stone, R.C. Srivyas, and M. Howard, "The left atrial appendage: our most lethal human attachment! Surgical implications," Eur J Cardiothorac Surg **17**(6), 718–722 (2000).
[6] A. Qureshi, O. Darwish, H. Chubb, S. Williams, D. Nechipurenko, F. Ataullakhanov, D. Nordsletten, O. Aslanidi, and A. De Vecchi, "Modelling Left Atrial Flow and Blood Coagulation for Risk of Thrombus Formation in Atrial Fibrillation," in *Computing in Cardiology 2020*, (IEEE, 2020).
[7] J.-J. Chiu, and S. Chien, "Effects of disturbed flow on vascular endothelium: pathophysiological basis and clinical perspectives," Physiol Rev **91**(1), 327–387 (2011).
[8] A.S. Wolberg, M.M. Aleman, K. Leiderman, and K.R. Machlus, "Procoagulant activity in hemostasis and thrombosis: Virchow's triad revisited," Anesth Analg **114**(2), 275–285 (2012).
[9] P. Di Achille, G. Tellides, C.A. Figueroa, and J.D. Humphrey, "A haemodynamic predictor of intraluminal thrombus formation in abdominal aortic aneurysms," Proceedings of the Royal Society A: Mathematical, Physical and Engineering Sciences **470**(2172), 20140163 (2014).
[10] M.I. Pons, J. Mill, A. Fernandez-Quilez, A.L. Olivares, E. Silva, T. de Potter, and O. Camara, "Joint Analysis of Morphological Parameters and In Silico Haemodynamics of the Left Atrial Appendage for Thrombogenic Risk Assessment," Journal of Interventional Cardiology **2022**(1), 9125224 (2022).
[11] R.G. Hart, O. Benavente, R. McBride, and L.A. Pearce, "Antithrombotic therapy to prevent stroke in patients with atrial fibrillation: a meta-analysis," Ann Intern Med **131**(7), 492–501 (1999).
[12] M. Salerno, B. Sharif, H. Arheden, A. Kumar, L. Axel, D. Li, and S. Neubauer, "Recent Advances in Cardiovascular Magnetic Resonance Techniques and Applications," Circ Cardiovasc Imaging **10**(6), e003951 (2017).
[13] S. Kozerke, J.M. Hasenkam, E.M. Pedersen, and P. Boesiger, "Visualization of flow patterns distal to aortic valve prostheses in humans using a fast approach for cine 3D velocity mapping," J Magn Reson Imaging **13**(5), 690–698 (2001).
[14] M. Markl, F.P. Chan, M.T. Alley, K.L. Wedding, M.T. Draney, C.J. Elkins, D.W. Parker, R. Wicker, C.A. Taylor, R.J. Herfkens, and N.J. Pelc, "Time-resolved three-dimensional phase-contrast MRI," J Magn Reson Imaging **17**(4), 499–506 (2003).
[15] D.N. Firmin, P.D. Gatehouse, J.P. Konrad, G.Z. Yang, P.J. Kilner, and D.B. Longmore, "Rapid 7-dimensional imaging of pulsatile flow," in *Proceedings of Computers in Cardiology Conference*, (1993), pp. 353–356.
[16] L. Wigström, L. Sjöqvist, and B. Wranne, "Temporally resolved 3D phase-contrast imaging," Magnetic Resonance in Medicine **36**(5), 800–803 (1996).
[17] M. Markl, D.C. Lee, N. Furiasse, M. Carr, C. Foucar, J. Ng, J. Carr, and J.J. Goldberger, "Left Atrial and Left Atrial Appendage 4D Blood Flow Dynamics in Atrial Fibrillation," Circulation: Cardiovascular Imaging **9**(9), e004984 (2016).
[18] J.U. Fluckiger, J.J. Goldberger, D.C. Lee, J. Ng, R. Lee, A. Goyal, and M. Markl, "Left atrial flow velocity distribution and flow coherence using four-dimensional FLOW MRI: A pilot study investigating the impact of age and Pre- and Postintervention atrial fibrillation on atrial hemodynamics," Journal of Magnetic Resonance Imaging **38**(3), 580–587 (2013).

[19] D.C. Lee, M. Markl, J. Ng, M. Carr, B. Benefield, J.C. Carr, and J.J. Goldberger, "Three-dimensional left atrial blood flow characteristics in patients with atrial fibrillation assessed by 4D flow CMR," European Heart Journal - Cardiovascular Imaging **17**(11), 1259–1268 (2016).
[20] W.V. Potters, P. van Ooij, H. Marquering, E. vanBavel, and A.J. Nederveen, "Volumetric arterial wall shear stress calculation based on cine phase contrast MRI," J Magn Reson Imaging **41**(2), 505–516 (2015).
[21] A. f. Stalder, M. f. Russe, A. Frydrychowicz, J. Bock, J. Hennig, and M. Markl, "Quantitative 2D and 3D phase contrast MRI: Optimized analysis of blood flow and vessel wall parameters," Magnetic Resonance in Medicine **60**(5), 1218–1231 (2008).
[22] A.J. Boyd, D.C.S. Kuhn, R.J. Lozowy, and G.P. Kulbisky, "Low wall shear stress predominates at sites of abdominal aortic aneurysm rupture," J Vasc Surg **63**(6), 1613–1619 (2016).
[23] N. Bappoo, M.B.J. Syed, G. Khinsoe, L.J. Kelsey, R.O. Forsythe, J.T. Powell, P.R. Hoskins, O.M.B. McBride, P.E. Norman, S. Jansen, D.E. Newby, and B.J. Doyle, "Low Shear Stress at Baseline Predicts Expansion and Aneurysm-Related Events in Patients With Abdominal Aortic Aneurysm," Circulation: Cardiovascular Imaging **14**(12), 1112–1121 (2021).
[24] D.N. Ku, D.P. Giddens, C.K. Zarins, and S. Glagov, "Pulsatile flow and atherosclerosis in the human carotid bifurcation. Positive correlation between plaque location and low oscillating shear stress," Arteriosclerosis: An Official Journal of the American Heart Association, Inc. **5**(3), 293–302 (1985).
[25] L.P. Parker, B. Reutersberg, M.B.J. Syed, B. Munshi, S. Richards, L.J. Kelsey, N. Sakalihasan, H.-H. Eckstein, P.E. Norman, and B.J. Doyle, "Proximal false lumen thrombosis is associated with low false lumen pressure and fewer complications in type B aortic dissection," Journal of Vascular Surgery **75**(4), 1181-1190.e5 (2022).
[26] A. Gonzalo, M. García-Villalba, L. Rossini, E. Durán, D. Vigneault, P. Martínez-Legazpi, O. Flores, J. Bermejo, E. McVeigh, A.M. Kahn, and J.C. del Alamo, "Non-Newtonian blood rheology impacts left atrial stasis in patient-specific simulations," International Journal for Numerical Methods in Biomedical Engineering **38**(6), e3597 (2022).
[27] R. Koizumi, K. Funamoto, T. Hayase, Y. Kanke, M. Shibata, Y. Shiraishi, and T. Yambe, "Numerical analysis of hemodynamic changes in the left atrium due to atrial fibrillation," J Biomech **48**(3), 472–478 (2015).
[28] J. Yang, C. Song, H. Ding, M. Chen, J. Sun, and X. Liu, "Numerical study of the risk of thrombosis in the left atrial appendage of chicken wing shape in atrial fibrillation," Front. Cardiovasc. Med. **9**, (2022).
[29] O. Mazumder, S. Gupta, D. Roy, and A. Sinha, "Computational Fluid Dynamic Model of Left Atrium to Analyze Hemodynamic Manifestation during Atrial Fibrillation," in *2022 44th Annual International Conference of the IEEE Engineering in Medicine & Biology Society (EMBC)*, (2022), pp. 3967–3971.
[30] T. Otani, A. Al-Issa, A. Pourmorteza, E.R. McVeigh, S. Wada, and H. Ashikaga, "A Computational Framework for Personalized Blood Flow Analysis in the Human Left Atrium," Ann Biomed Eng **44**(11), 3284–3294 (2016).
[31] M. García-Villalba, L. Rossini, A. Gonzalo, D. Vigneault, P. Martinez-Legazpi, O. Flores, and J.C. del Álamo, "Demonstration of Patient-Specific Simulations to Assess Left Atrial Appendage Thrombogenesis Risk," Front. Physiol. **12**, (2021).
[32] A. Masci, M. Alessandrini, D. Forti, F. Menghini, L. Dedé, C. Tomasi, A. Quarteroni, and C. Corsi, "A Proof of Concept for Computational Fluid Dynamic Analysis of the Left Atrium in Atrial Fibrillation on a Patient-Specific Basis," Journal of Biomechanical Engineering **142**(011002), (2019).

[33] M. Garreau, T. Puiseux, S. Toupin, D. Giese, S. Mendez, F. Nicoud, and R. Moreno, "Accelerated sequences of 4D flow MRI using GRAPPA and compressed sensing: A comparison against conventional MRI and computational fluid dynamics," Magn Reson Med **88**(6), 2432–2446 (2022).
[34] A. Fedorov, S. Khallaghi, C.A. Sánchez, A. Lasso, S. Fels, K. Tuncali, E.N. Sugar, T. Kapur, C. Zhang, W. Wells, P.L. Nguyen, P. Abolmaesumi, and C. Tempany, "Open-source image registration for MRI-TRUS fusion-guided prostate interventions," Int J Comput Assist Radiol Surg **10**(6), 925–934 (2015).
[35] S. Klein, M. Staring, K. Murphy, M.A. Viergever, and J.P.W. Pluim, "elastix: A Toolbox for Intensity-Based Medical Image Registration," IEEE Transactions on Medical Imaging **29**(1), 196–205 (2010).
[36] D.P. Shamonin, E.E. Bron, B.P.F. Lelieveldt, M. Smits, S. Klein, and M. Staring, "Fast Parallel Image Registration on CPU and GPU for Diagnostic Classification of Alzheimer's Disease," Front. Neuroinform. **7**, (2014).
[37] S. Chien, "Biophysical Behavior of Red Cells in Suspensions," in *The Red Blood Cell,* (Academic, New York, 1975), pp. 1031–1133.
[38] D. Du BOIS, and E.F. Du BOIS, "Clinical Calorimetry: Tenth Paper A Formula to Estimate the Approximate Surface Area if Height and Weight Be Known," Archives of Internal Medicine **XVII**(6_2), 863–871 (1916).
[39] S. Petersson, P. Dyverfeldt, and T. Ebbers, "Assessment of the accuracy of MRI wall shear stress estimation using numerical simulations," J Magn Reson Imaging **36**(1), 128–138 (2012).
[40] S. Wessler, "Thrombosis in the presence of vascular stasis," The American Journal of Medicine **33**(5), 648–666 (1962).
[41] R. Virchow, *Gesammelte Abhandlungen zur wissenschaftlichen Medicin* (Grote, 1862).
[42] M. Spartera, G. Pessoa-Amorim, A. Stracquadanio, A. Von Ende, A. Fletcher, P. Manley, S. Neubauer, V.M. Ferreira, B. Casadei, A.T. Hess, and R.S. Wijesurendra, "Left atrial 4D flow cardiovascular magnetic resonance: a reproducibility study in sinus rhythm and atrial fibrillation," Journal of Cardiovascular Magnetic Resonance **23**(1), 29 (2021).
[43] G.M. Bosi, A. Cook, R. Rai, L.J. Menezes, S. Schievano, R. Torii, and G.B. Burriesci, "Computational Fluid Dynamic Analysis of the Left Atrial Appendage to Predict Thrombosis Risk," Frontiers in Cardiovascular Medicine **5**, 34–34 (2018).
[44] B.M. Fanni, K. Capellini, M. Di Leonardo, A. Clemente, E. Cerone, S. Berti, and S. Celi, "Correlation between LAA Morphological Features and Computational Fluid Dynamics Analysis for Non-Valvular Atrial Fibrillation Patients," Applied Sciences **10**(4), 1448 (2020).
[45] L. Wang, Z. Wang, R. Fang, and Z.-Y. Li, "Evaluation of Stroke Risk in Patients With Atrial Fibrillation Using Morphological and Hemodynamic Characteristics," Front. Cardiovasc. Med. **9**, (2022).
[46] J. Lantz, V. Gupta, L. Henriksson, M. Karlsson, A. Persson, C.-J. Carlhäll, and T. Ebbers, "Impact of Pulmonary Venous Inflow on Cardiac Flow Simulations: Comparison with In Vivo 4D Flow MRI," Ann Biomed Eng **47**(2), 413–424 (2019).
[47] E. Durán, M. García-Villalba, P. Martínez-Legazpi, A. Gonzalo, E. McVeigh, A.M. Kahn, J. Bermejo, O. Flores, and J.C. del Álamo, "Pulmonary vein flow split effects in patient-specific simulations of left atrial flow," Computers in Biology and Medicine **163**, 107128 (2023).
[48] M. Habibi, J.A.C. Lima, I.M. Khurram, S.L. Zimmerman, V. Zipunnikov, K. Fukumoto, D. Spragg, H. Ashikaga, J. Rickard, J.E. Marine, H. Calkins, and S. Nazarian, "Association of Left Atrial Function and Left Atrial Enhancement in Patients With Atrial Fibrillation," Circulation: Cardiovascular Imaging **8**(2), e002769 (2015).

[49] E. Donal, R. Ollivier, D. Veillard, S. Hamonic, D. Pavin, J.-C. Daubert, and P. Mabo, "Left atrial function assessed by trans-thoracic echocardiography in patients treated by ablation for a lone paroxysmal atrial fibrillation," European Journal of Echocardiography **11**(10), 845–852 (2010).
[50] J. Mill, J. Harrison, M. Saiz-Vivo, C. Albors, X. Morales, A.L. Olivares, X. Iriart, H. Cochet, J. Noailly, M. Sermesant, and O. Camara, "The role of the pulmonary veins on left atrial flow patterns and thrombus formation," Sci Rep **14**(1), 5860 (2024).
[51] A. Masci, L. Barone, L. Dedè, M. Fedele, C. Tomasi, A. Quarteroni, and C. Corsi, "The Impact of Left Atrium Appendage Morphology on Stroke Risk Assessment in Atrial Fibrillation: A Computational Fluid Dynamics Study," Front. Physiol. **9**, (2019).
[52] D. Dillon-Murphy, D. Marlevi, B. Ruijsink, A. Qureshi, H. Chubb, E. Kerfoot, M. O'Neill, D. Nordsletten, O. Aslanidi, and A. de Vecchi, "Modeling Left Atrial Flow, Energy, Blood Heating Distribution in Response to Catheter Ablation Therapy," Front. Physiol. **9**, (2018).
[53] H.A. Kjeldsberg, C. Albors, J. Mill, D.V. Medel, O. Camara, J. Sundnes, and K. Valen-Sendstad, "Impact of left atrial wall motion assumptions in fluid simulations on proposed predictors of thrombus formation," International Journal for Numerical Methods in Biomedical Engineering **40**(6), e3825 (2024).
[54] N. Paliwal, H.-C. Park, Y. Mao, S.J. Hong, Y. Lee, D.D. Spragg, H. Calkins, and N.A. Trayanova, "Slow blood-flow in the left atrial appendage is associated with stroke in atrial fibrillation patients," Heliyon **10**(5), e26858 (2024).
[55] J.M. Lee, J. Seo, J.-S. Uhm, Y.J. Kim, H.-J. Lee, J.-Y. Kim, J.-H. Sung, H.-N. Pak, M.-H. Lee, and B. Joung, "Why Is Left Atrial Appendage Morphology Related to Strokes? An Analysis of the Flow Velocity and Orifice Size of the Left Atrial Appendage," J Cardiovasc Electrophysiol **26**(9), 922–927 (2015).
[56] G.I. Grigoriadis, A.I. Sakellarios, I. Kosmidou, K.K. Naka, C. Ellis, L.K. Michalis, and D.I. Fotiadis, "Wall shear stress alterations at left atrium and left atrial appendage employing abnormal blood velocity profiles," in *2020 42nd Annual International Conference of the IEEE Engineering in Medicine & Biology Society (EMBC)*, (2020), pp. 2565–2568.
[57] T. Ito, and M. Suwa, "Assessment of left atrial appendage function by echocardiography," Heart Fail Rev **28**(5), 1177–1187 (2023).
[58] M.M. Bissell, F. Raimondi, L. Ait Ali, B.D. Allen, A.J. Barker, A. Bolger, N. Burris, C.-J. Carhäll, J.D. Collins, T. Ebbers, C.J. Francois, A. Frydrychowicz, P. Garg, J. Geiger, H. Ha, A. Hennemuth, M.D. Hope, A. Hsiao, K. Johnson, S. Kozerke, L.E. Ma, M. Markl, D. Martins, M. Messina, T.H. Oechtering, P. van Ooij, C. Rigsby, J. Rodriguez-Palomares, A.A.W. Roest, A. Roldán-Alzate, S. Schnell, J. Sotelo, M. Stuber, A.B. Syed, J. Töger, R. van der Geest, J. Westenberg, L. Zhong, Y. Zhong, O. Wieben, and P. Dyverfeldt, "4D Flow cardiovascular magnetic resonance consensus statement: 2023 update," J Cardiovasc Magn Reson **25**(1), 1–24 (2023).
[59] S. Bäck, L. Henriksson, A.F. Bolger, C.-J. Carlhäll, A. Persson, M. Karlsson, and T. Ebbers, "Assessment of transmitral and left atrial appendage flow rate from cardiac 4D-CT," Commun Med (Lond) **3**, 22 (2023).
[60] L. Ma, J. Yerly, L. Di Sopra, D. Piccini, J. Lee, A. DiCarlo, R. Passman, P. Greenland, D. Kim, M. Stuber, and M. Markl, "Using 5D flow MRI to decode the effects of rhythm on left atrial 3D flow dynamics in patients with atrial fibrillation," Magn Reson Med **85**(6), 3125–3139 (2021).